Assessing the correlation between mutant rhodopsin stability and the severity of retinitis pigmentosa

Richard McKeone,[1,3] Matthew Wikstrom,[2,3] Christina Kiel,[4,5] P. Elizabeth Rakoczy[3]

[1]*Department of Molecular Ophthalmology, Lions Eye Institute, Perth, Western Australia;* [2]*Centre for Experimental Immunology, Lions Eye Institute, Perth, Western Australia;* [3]*Centre for Ophthalmology and Visual Science, University of Western Australia, Perth, Western Australia;* [4]*EMBL/CRG Systems Biology Research Unit, Centre for Genomic Regulation (CRG), Dr. Aiguader 88, 08003 Barcelona, Spain;* [5]*Universitat Pompeu Fabra (UPF), 08003 Barcelona, Spain*

Purpose: Following a previous study that demonstrated a correlation between rhodopsin stability and the severity of retinitis pigmentosa (RP), we investigated whether predictions of severity can be improved with a regional analysis of this correlation. The association between changes to the stability of the protein and the relative amount of rhodopsin reaching the plasma membrane was assessed.

Methods: Crystallography-based estimations of mutant rhodopsin stability were compared with descriptions in the scientific literature of the visual function of mutation carriers to determine the extent of associations between rhodopsin stability and clinical phenotype. To test the findings of this analysis, three residues of a green fluorescent protein (GFP) tagged rhodopsin plasmid were targeted with site-directed random mutagenesis to generate mutant variants with a range of stability changes. These plasmids were transfected into HEK-293 cells, and then flow cytometry was used to measure rhodopsin on the cells' plasma membrane. The GFP signal was used to measure the ratio between this membrane-bound rhodopsin and total cellular rhodopsin. FoldX stability predictions were then compared with the surface staining data and clinical data from the database to characterize the relationship between rhodopsin stability, the severity of RP, and the expression of rhodopsin at the cell surface.

Results: There was a strong linear correlation between the scale of the destabilization of mutant variants and the severity of retinal disease. A correlation was also seen in vitro between stability and the amount of rhodopsin at the plasma membrane. Rhodopsin is drastically reduced on the surface of cells transfected with variants that differ in their inherent stability from the wild-type by more than 2 kcal/mol. Below this threshold, surface levels are closer to those of the wild-type.

Conclusions: There is a correlation between the stability of rhodopsin mutations and disease severity and levels of membrane-bound rhodopsin. Measuring membrane-bound rhodopsin with flow cytometry could improve prognoses for poorly characterized mutations and could provide a platform for measuring the effectiveness of treatments.

The majority of the more than 130 rhodopsin point mutations that have been discovered to date in humans [1] cause autosomal dominant retinitis pigmentosa (adRP). This degenerative disease of the retina usually begins with night blindness and progresses to peripheral vision loss and in the most severe cases to loss of central vision and total blindness. There is a large variability in the severity of rhodopsin-associated retinitis pigmentosa (RP). Some individuals experience night blindness, poor visual acuity, and reduced visual field soon after birth and can be completely blind by the time they reach their fourth decade of life [2] whereas others retain useful vision into at least their ninth decade [3]. Severity is heavily influenced by the specific identity of the mutant allele, although environmental, dietary, and genetic cofactors are also likely to contribute [4].

After rhodopsin is synthesized in the rough endoplasmic reticulum, it is transported to the plasma membrane of the inner segment before traversing the cilia and forming endocytosed vesicles at the base of the outer segments that develop into the nascent discs [5,6]. The extracellular portion of the membrane-bound protein therefore becomes the intradiscal portion in rod discs. Cell culture lines such as HEK-293 and COS-7 have been used intensively to model the mutations that affect the preciliary transport and interactions with the chromophore 11-cis retinal [7-10]. In these models, the rhodopsin that is transported to the plasma membrane does not form discs, and thus, the intradiscal portion of the molecule can also be referred to as the extracellular region in this context.

Shortly after the first rhodopsin mutation was discovered [11], work by Sung and Nathans et al. [9,10] and the Khorana laboratory [12] revealed a clear division between two groups of rhodopsin mutations. Sung classified class I mutations as those that resemble the wild-type in yield, efficiency of regeneration with 11-cis-retinal, and in subcellular

Correspondence to: Elizabeth Rakoczy, Lions Eye Institute, 6 Verdun St, Nedlands, WA 6009, Australia: Phone: +618 9381 0726; FAX:+618 9381 0739, email: elizabeth.rakoczy@uwa.edu.au
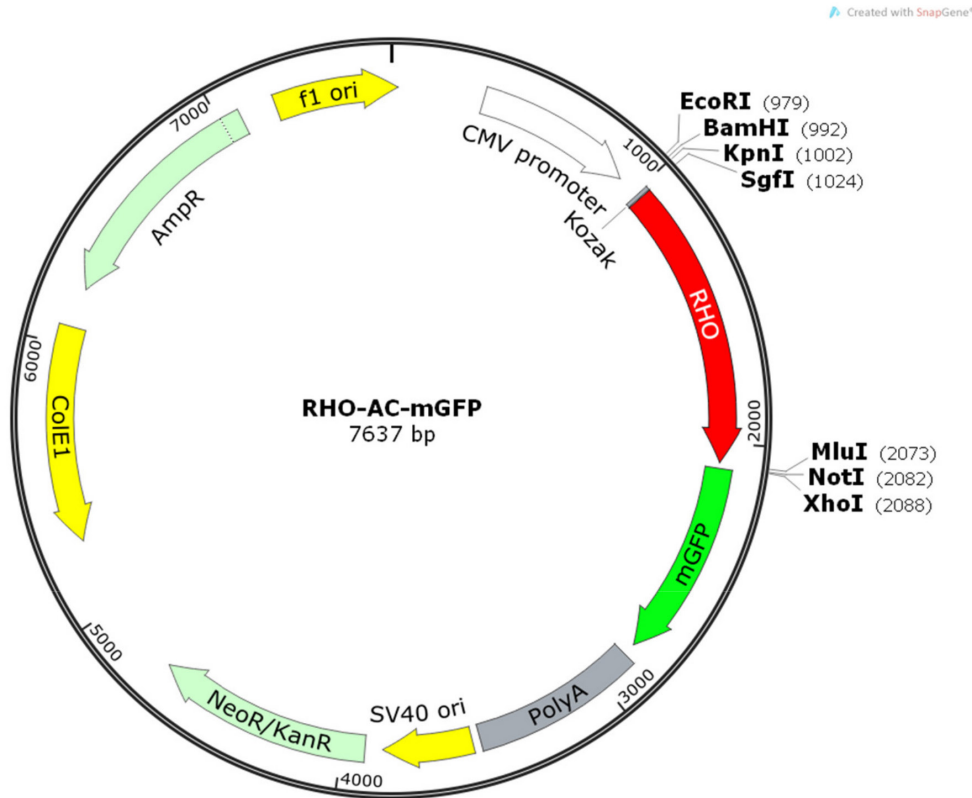
Figure 1. Map of the RHO-AC-mGFP plasmid. The restriction enzymes Sgf I and Mlu I were used to extract the rhodopsin ORF from plasmid RC211328 and insert it into the vector pCMV6-AC-mGFP (Map constructed using SnapGene®, GSL Biotech; snapgene.com).

localization, but do not reach the outer segment [13,14]. Class II mutations in contrast, accumulate at low levels, regenerate poorly with 11-cis-retinal, and are inefficiently transported to the plasma membrane [8,12,15,16]. Mendes later collated evidence from several other laboratories to further extend the biochemical classification [17] to differentiate mutations that affect endocytosis (class III) [18], that affect rod-opsin stability and post-translational modification [19] (class IV), that show an increased rate of transducin activation [20] (class V), and that induce constitutive opsin activation (class VI) [21].

The most common reason why class II mutants fail to integrate with the plasma membrane is because they are retained at the endoplasmic reticulum [10]. This organelle is essential for the correct folding of proteins and plays a critical role in numerous other aspects of post-translational processing. The physical association between proteinaceous aggregate and molecular chaperones in cells transfected with class II mutants [22] is convincing evidence that these mutant rhodopsins are retained by misfolding. A characterization of the way that alterations to rhodopsin stability can lead to aberrant folding is thus critical for a deeper understanding of the mechanisms behind this process. Several recent technologies have the potential to facilitate this.

One such tool is the algorithm FoldX [23], which was used for a systematic meta-analysis of rhodopsin mutant

Mutation	Night blindness Onset	Daytime Vision Loss Onset	Visual Acuity	V/4 Visual Field
T4K	1	2	2	2
N15S	2	4	3	-
T17M	7	8	8	3
V20G	-	1	1	-
P23A	3	4	6	2
P23H	22	34	40	33
G106R	1	9	6	1
G109R	1	-	-	-
P171Q	1	1	-	-
S176F	2	2	2	1
G182S	2	2	2	1
C187Y	2	7	3	7
D190N	3	3	2	-
D190Y	2	1	2	-
T193M	-	1	-	-

TABLE 1. NUMBER OF INDIVIDUALS WITH CLINICAL PHENOTYPING DATA FOR EACH FOLD-X COMPATIBLE MUTATION.

Number of individuals with intradiscal mutations with available clinical data that fitted the criteria of the meta-analysis.

stability that highlighted a correlation between stability change and disease symptom severity [24]. FoldX has been experimentally validated with 1,088 mutations in 20 proteins within most of the structural environments that occur in proteins [25] and is currently available as FoldX v3.0 beta3. Previous stability predictions have shown a good correlation with experimental data [26], and correlations have been identified between stability estimations and the severity of several conditions [24,27,28], including other visual diseases [24,29-31].

The presence of insoluble aggregates in some class II mutations has led to comparisons with other dominant neurodegenerative conditions such as Parkinson's and Alzheimer's disease [32]. These misfolding diseases are thought to cause disease by toxic gain of function effects, and there are many similarities between these diseases and rhodopsin-associated RP, including the formation of ubiquitinated aggresomes, the recruitment of cellular chaperones, and the accrual of insoluble aggregates [8]. However, evidence from mice [15,33] and cell cultures [32] suggests that dominant-negative effects can also result from the destabilizing class II rhodopsin mutations [34]. One possible explanation is that in these cases, the misfolded protein retains an active dimerization motif so the wild-type/mutant heterodimers lose their functionality. Because dimerization in heterozygous individuals can

incorporate such heterodimers as well as homodimers, the level of functional wild-type dimer may be reduced below the level that would be seen in the phenotypically normal heterozygote nulls and below the required threshold for normal gene function [17]. The known links between destabilization and misfolding [35] and between misfolding and cellular localization [36] led us to investigate whether there is a direct correlation between surface rhodopsin and stability that could contribute to the severity correlation observed for the misfolding mutations that are categorized for rhodopsin as class II mutations.

A more detailed examination of the correlations between stability, structure, and clinical phenotypes in a subgroup of class II mutations is expected to provide unique insight into the traits associated with these mutations. This is an exciting prospect given the potential for improvements in disease prognosis and the possibility of building a basic framework on which to assess amenability to rhodopsin treatments. Our aim in this investigation was to investigate the correlation between the stability of class II rhodopsin mutations and four parameters that can be used to determine ocular health in patients with RP: visual acuity, visual field, night blindness onset, and daytime vision loss onset.
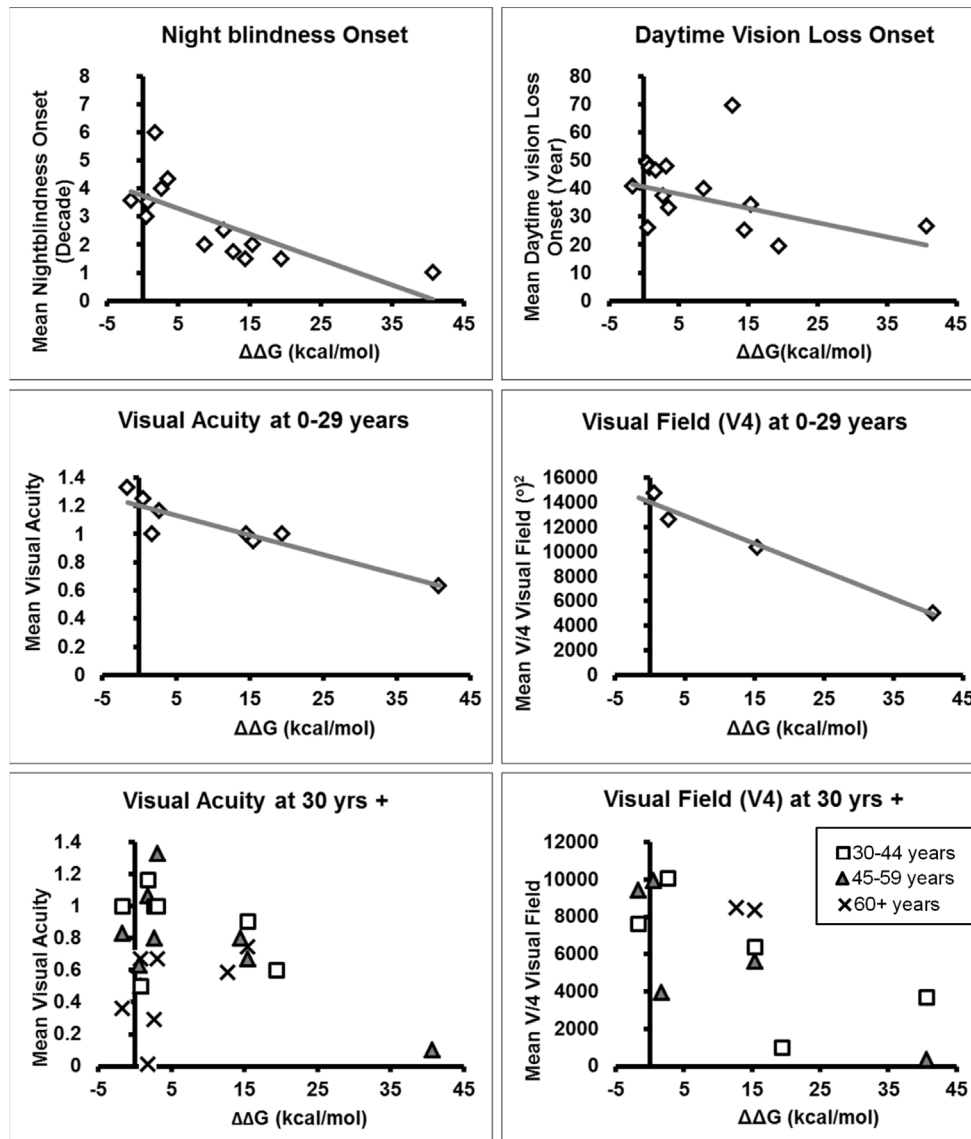
Figure 2. Correlation between retinitis pigmentosa severity and rhodopsin stability. The relationship between the age of onset and the stability of rhodopsin variants with mutations in intradiscal residues is shown (top). There is a strong correlation between ΔΔG and the severity of visual function in the youngest cohort (0–29 years, center), but in the older cohorts, other factors play an increasingly influential role in clinical severity, and the correlation is reduced or completely masked (bottom).

METHODS

Disease prediction and the statistical analysis of clinical phenotype data: Clinical data was obtained by data-mining the available literature as described previously [24]. Stability calculations were based on the FoldX estimations of the free energy of unfolding (ΔG) of the rhodopsin protein. ΔΔG is the difference between the stability of a mutant rhodopsin variant and the wild-type. Rhodopsin calculations of ΔG were made with the bovine form of the molecule [37]. Bovine rhodopsin differs from human rhodopsin by only three positions within the amino acid sequence: Met216 in human rhodopsin is a leucine in the bovine sequence, human Ser270 is replaced by a glycine, and human Ser297 is replaced by a threonine. Each of these inter-species variations is predicted to have negligible

effects on the molecule by FoldX and Sorting Intolerant From Tolerant (SIFT) [24], and the bovine rhodopsin structure has been used by many authors as a model of mammalian rhodopsin with immediate relevance to human disease owing to its high level of functional and sequence homology [38-40]. Thus, we believed the stability predictions derived from modeling mutations of the bovine structures were likely to closely represent mutations of human rhodopsin. FoldX data for the human disease mutation meta-analysis has been published previously [24], but the regression analysis in that case was performed on a functional basis. Here, we first grouped the mutations into their respective regions (intradiscal, cytoplasmic, transmembrane helix facing, transmembrane lipid facing, and retinal binding zone) before we analyzed the correlations with phenotype severity.

Mutation	ΔΔG FoldX (kcal/mol)	Night blindness onset (decade)	Daytime vision loss onset (yr)	Source References
T4K	0.592	3.0	26.0	[59]
N15S	0.818	3.5	47.3	[60]
T17M	−1.616	3.6	40.9	[61-64]
V20G	3.186	ND	48.0	[65]
P23A	2.712	4.0	37.4	[66]
P23H	15.47	2.0	34.4	[11,41,42,67,68]
G106R	1.778	6.0	46.4	[69-71]
G109R	11.394	2.5	ND	[72]
P171Q	8.686	2.0	40.0	[73]
S176F	19.452	1.5	19.5	[65]
G182S	12.786	1.8	75.0	[62]
C187Y	40.692	1.0	26.4	[2]
D190N	3.618	4.3	33.0	[74]
D190Y	14.49	1.5	25.0	[74]
T193M	0.464	ND	49.0	[75]

Mean onset age for each intra-discal mutation. Daytime vision loss onset describes when patients first noticed a deterioration in their visual acuity or visual field, or when such a deterioration was first observed by their practitioner. Night blindness onset and daytime vision are presented in different units (decade and year respectively) due to the respective units quoted in the literature. ND=No data.

The other parameters used for our meta-analysis have been outlined previously [24], but for ease of interpretation, a summary of the inclusion criteria and additional details to clarify the methods are presented here. The age at which visual acuity or visual field was first reported to deteriorate was combined into the single parameter of "onset of daytime vision loss." In cases where data for the age of visual field or visual acuity loss were not available, daytime vision loss has also been inferred from what were described in the source papers as the onset age of symptoms "other than night blindness," or when electroretinography readings showed that cones as well as rods were severely reduced. Patients who could perceive only counting fingers, hand motion, or light were all given a visual acuity score of 0. The majority of sources clarified that visual acuity was assessed with best-corrected vision; whereas no sources specified that visual acuity testing was without correction. We therefore included all visual acuity measurements, assuming that they were taken with best corrected vision. Goldmann perimetry tests with isopters of V/4 were used to assess visual fields. Visual field data were either quoted in the original sources as the angle of constriction, the extent of the visual field loss in degrees squared ((°)²) [41], percentage of the normal visual field [42,43], or by perimetry charts. Visual field references that used "% of normal" were converted to visual field measurements using baselines derived from a previous study of normal peripheral isopter positions [44]. Perimetry chart data were converted to visual field measurements with the software Image J [45].

Regression analysis (using Excel Analysis ToolPak, Excel 2010; Microsoft, Redmond, WA) of RP clinical severity and the relative stabilities of different rhodopsin mutations was performed on a regional basis, with the molecule separated into five structural regions: intradiscal, transmembrane helix facing, transmembrane lipid facing, retinal binding zone, and cytoplasmic. This was repeated for visual acuity and visual field, but these parameters are known to be influenced by age; therefore, the data were controlled for age by the inclusion of an "age" parameter in a multiple linear regression analysis.

The RHO-AC-monomeric green fluorescent protein plasmid: To obtain an objective measure of surface rhodopsin, a plasmid that expresses human rhodopsin fused to a monomeric green fluorescent protein (GFP) was used. GFP tags at the C-terminus do not appear to have any effect on the intracellular transport of rhodopsin within non-ciliated, cultured cells [7,8]; but previous reports have shown that fusion proteins containing rhodopsin and enhanced green fluorescent protein are not trafficked correctly in rod cells [46-49]. We speculated that such aberrant trafficking may be

exacerbated by the tendency for GFP to dimerize, and since there are several palmitoylation sites near the C-terminus, we wanted to avoid interference with such critical processes so replaced the dimerizing GFP with monomeric GFP. The Rhodopsin ORF was sub-cloned by Origene from plasmid RC211328 into the vector pCMV6-AC-mGFP to produce the custom-built vector RHO-AC-mGFP (Figure 1).

Site-directed random mutagenesis: Site-directed random mutagenesis was performed with random bases at the codons P23, G106, and D190, using a method based on the mutagenesis approach described by Sanchis et al. [50]. The thermal conditions for site-directed random mutagenesis PCR were as follows: 98 °C for 2 min; and then 5 cycles of 98 °C for 10 s, 56 °C–67 °C for 30 s, 72 °C for 1.75 min. This was followed by 20 cycles of 98 °C for 10 s and 72 °C for 30 s or 72 °C for 2.5 min and then a 5 min extension at 72 °C. The 50 µl reaction volume contained 0.2 mM dNTPs, 1 µl F and R primers (5 pmol), 50 ng template, 0.5 µl Phusion DNA Polymerase, Thermo Scientific (Waltham, MA), 1X of the reaction buffer that was supplied with the polymerase. The forward primer sequences were 5′-GTG GAA TCN NKT ACT ACA CGC TCA-3′ for D190 mutagenesis; 5′-GCA GCN NKT TCG AGT ACC CAC-3′ for P23 mutagenesis; and 5′-GAT ACT TCG TCT TCN NKC CCA C-3′ for G106 mutagenesis. The reverse primer for all three reactions was 5′-ACG TCG TGA CTG GGA AAA CC-3′. The three forward primers contained the NNK degenerate base sequence, which randomized the resulting product at the loci of interest. Potential mutant rhodopsin plasmids were sequenced to determine the identity of the mutations.

FoldX analysis: FoldX data for human mutation analysis had been published previously [24], but further analysis of the three target residues that underwent site-directed mutagenesis was required. One of the main barriers to accurately predicting protein stability are errors within the structural template. Therefore, one should always model mutations of interest on several template structures. In our earlier analysis, we used five template structures, which mostly resulted in similar energy predictions. We predicted the effects of all possible mutations at the three positions targeted for site-directed mutagenesis, using these original five template structures as well as the respective second chains from four of the crystallographic units. We thus obtained the average and standard deviations (after removing two outliers) from nine PDB structures.

Cell culture: HEK-293 cells at a passage number of between 38 and 50 were seeded at 300 cells/mm² in DMEM (Gibco® - Life Technologies, Carlsbad, CA) media into wells of a 24-well plate. Several earlier studies used HEK-293 cells for rhodopsin expression studies, and evidence suggests that the majority of rhodopsin has a native conformation in these cells [10,51]. After the cells were incubated for 48 h at 37 °C in 5% CO_2, the RHO-AC-mGFP plasmid was transfected into the cells using X-treme gene HP transfection reagent (Roche, Basel, Switzerland) at a ratio of 1 µl transfection reagent to 1 µg of RHO-AC-mGFP DNA in 100 µl of serum-free DMEM media. 50 µl of this transfection mixture was transferred to each well. Untagged rhodopsin controls were transfected using the same conditions as the tagged constructs, but with the rhodopsin plasmid RHO-SC300090 (Origene, Rockville, MD).

TABLE 3. VISUAL ACUITY.					
Mutation	**0–29 years**	**30–44 years**	**45–59 years**	**60+ Years**	**Source References**
T4K	1.25	ND	0.63	ND	[59]
N15S	ND	0.50	0.50	0.67	[60,76]
T17M	1.33	1.00	0.83	0.36	[61-64]
V20G	ND	1.00	1.33	0.67	[65]
P23A	1.17	1.00	0.80	0.29	[66]
P23H	0.95	0.91	0.67	0.74	[41,42,67,68]
G106R	1.00	1.17	1.07	0.01	[69,70]
S176F	1.00	0.60	ND	ND	[65]
G182S	ND	ND	ND	0.59	[62]
C187Y	0.63	ND	0.10	ND	[2]
D190N	ND	ND	1.30	ND	[74]
D190Y	1.00	ND	0.80	ND	[74]

Mean visual acuity data (converted to decimal notation) for each intra-discal mutation within the age subgroups. ND=No data.

	TABLE 4. V/4 VISUAL FIELD.				
Mutation	0–29years	30–44years	45–59years	60+years	Source References
T4K	14,736	ND	9936	ND	[59]
T17M	ND	7622	9423	ND	[62-64]
P23A	12,563	10,052	ND	ND	[66]
P23H	10,330	6360	5598	8335	[41,42,68]
G106R	ND	ND	3935	ND	[69,70]
S176F	ND	1001	ND	ND	[65]
G182S	ND	ND	ND	8465	[62,77]
C187Y	4998	3691	345	ND	[2]

Mean visual field data $(°)^2$ for each intra-discal mutation within age sub-groups. ND=No data.

Flow cytometry: Forty hours after transfection, cells were washed once in PBS (136.9 mM NaCl, 2.7 mM KCl, 8.1 mM Na_2HPO_4, 1.5 mM KH_2PO_4). They were then disassociated from the vessel surface by covering with 50 µl trypsin and incubated for 4 min at 37 °C. Cells were then resuspended with 150 µl DMEM media and centrifuged at 400 ×*g* for 4 min, washed by resuspension and centrifugation in PBS, and then resuspended and fixed in 4% paraformaldehyde in PBS for 20 min. After two more PBS washes, a blocking solution containing 3% bovine serum albumin in PBS was added to the cells before anti-rhodopsin RET-P1 monoclonal antibody was added (Sigma-Aldrich, St Louis, MO) at a dilution of 1:2,000 and incubated on ice for 1 h. The RET-P1 antibody recognizes amino acids 4–10 at rhodopsin's N-terminus and is therefore detected under non-permeabilizing conditions in which no detergents have been added at any stage of sample preparation. The cells were washed twice before APC-Cy7 conjugated goat anti-mouse antibody was added at a dilution of 1:2,000. Further incubation at 30 min on ice was followed by two washes and resuspension in 200 µl PBS for analysis. The Ret-P1 gate was set according to the wavelength at which there were negligible numbers of cells in the secondary antibody control.

Immunohistochemistry: The culture conditions and time frames for immunohistochemistry were identical to those used for flow cytometry except that the cells were grown on 0.7 cm² eight-chamber slides (Becton Dickinson, Franklin Lakes, NJ) and were transfected with 30 µl transfection mix. Washes were performed by adding 500 µl PBS to each chamber, followed by 5 min at room temperature. The secondary antibody for microscopy was donkey anti-mouse conjugated with Alexa Fluor 568 (Molecular Probes, Eigene, OR). Image analysis of fluorescence microscopy photographs was performed using ImageJ [45] using the following procedure: Fluorescence intensity thresholds for the GFP signal were selected using wild-type images, to limit the regions of interest to cells that were actively producing the RHO-GFP fusion product. The selected areas for each GFP image were then applied to the AF568 antibody image from the equivalent view field. Background grayscale measurements were subtracted from the grayscale measurements of the GFP+ cells, before the red/green ratio was determined.

Confocal microscopy was performed using a Nikon Ti-E inverted microscope with a Nikon A1Si spectral detector. Cells analyzed with confocal microscopy were labeled with biotinylated antimouse CD44 (Biolegend, San Diego, CA) and streptavidin conjugated to Alexa Fluor 594.

Statistical analysis: Regression analysis of the human clinical data was performed using the Microsoft Excel data analysis toolkit. ANOVA and the Tukey-Kramer post-hoc test were performed using GB-Stat (v9.0).

RESULTS

Data analysis of phenotypic data: Our original analysis of the clinical phenotype data identified a correlation between the means of the daytime vision loss onset and ΔΔG when all non-functional residues were analyzed [24]. The new analysis here, in contrast, takes all available data into account individually rather than only the mutational means, and highlights several additional correlations in addition to identifying the region with the strongest correlation. Carriers of mutations within the intradiscal region of rhodopsin (Table 1) retain a highly significant correlation under the new analytical parameters (see Figure 2, Table 2). For every ΔΔG increase of 1 kcal/mol, there was a decrease in the age of onset of night blindness of 0.9 years ($p < 0.0001$, $R^2 = 0.3$), a decrease in the onset of daytime vision loss of 0.5 years ($p = 0.008$, $R^2 = 0.1$); a decrease in visual acuity of 0.009 ($p = 0.007$, $R^2 = 0.3$; Figure 2, Table 3), and a decrease in visual field of $180(°)^2$ ($p = 0.003$,

R^2=0.2; Figure 2, Table 4). In contrast to the intradiscal residues, the transmembrane, cytoplasmic, and retinal-zone residues showed no correlation between stability change and visual function.

Although highly significant, the intradiscal residue correlations were associated with low R square values by the standards of other correlative studies due to variability between individuals with the same mutation. These data suggest that there is a genuine correlation between energy change and disease severity, but the increased consistency and strength of correlation in the intradiscal region compared to the other regions should be emphasized.

As expected, the multiple linear regression analysis showed that there was also a strong association between increasing age and decreasing visual acuity ($p=5.5\times10^{-7}$), but the association between age and visual field deterioration was marginal (p=0.05 for the V/4 isopter data).

In vitro analysis: To determine whether the correlation between rhodopsin stability and RP severity was due to reduced efficiency of its transport to the plasma membrane, we aimed to quantify the levels of surface rhodopsin. Three residues (G106, D190, and P23) were selected for mutagenesis because of their position on the intradiscal region of the protein (Figure 3) and because they are associated with multiple pathogenic mutations in the human population. A series of mutations were generated and the relevant ΔG values calculated (Figure 4).

Cell dissociation methods were optimized for maximum antibody signal intensity. Citric saline was compared with EDTA and trypsin. Previous reports have shown that any one of these substances can be used to dissociate cell monolayers for flow cytometry [52]. Our tests showed that the strongest APC-Cy7 signal was observed in the trypsinized cells.

Population density gradients showed that within cells transfected with wild-type rhodopsin, the intensity of GFP expression correlated closely with the intensity of APC-Cy7 detection (Figure 5A). In mutant variants though, as well as an overall reduction in APC-Cy7 signal intensity, there is a wider range of APC-Cy7 intensities in GFP+ cells (Figure 5B).

Mutations that resulted in a high ΔΔG were associated with a noticeable drop in levels of detectable surface rhodopsin, whereas variants with low ΔΔG had a milder effect (Figure 6A and Table 5). ANOVA of the RET-1/APC-cy7 signal from the GFP+ transfected cells, followed by a Tukey-Kramer post-hoc test showed a significant elevation (p<0.01) of the wild-type ($1320.8_{RFI} \pm339.9$) compared to any of the mutant variants (mutant means ranged from $337.4_{RFI} \pm90.6$ SD for G106R to $70.9_{RFI} \pm10.2$ SD for P23N). Reanalysis following the normalization of these means to the mutant/wild-type ratio revealed that G106R was significantly elevated (p<0.01) above all of the other mutant variants (G106R=0.259±0.05 SD) and D190N was significantly higher than all but one (D190P; p<0.05) of the other mutations (D190n=0.153±0.02 SD; D190p=0.106 ±0.04 SD;
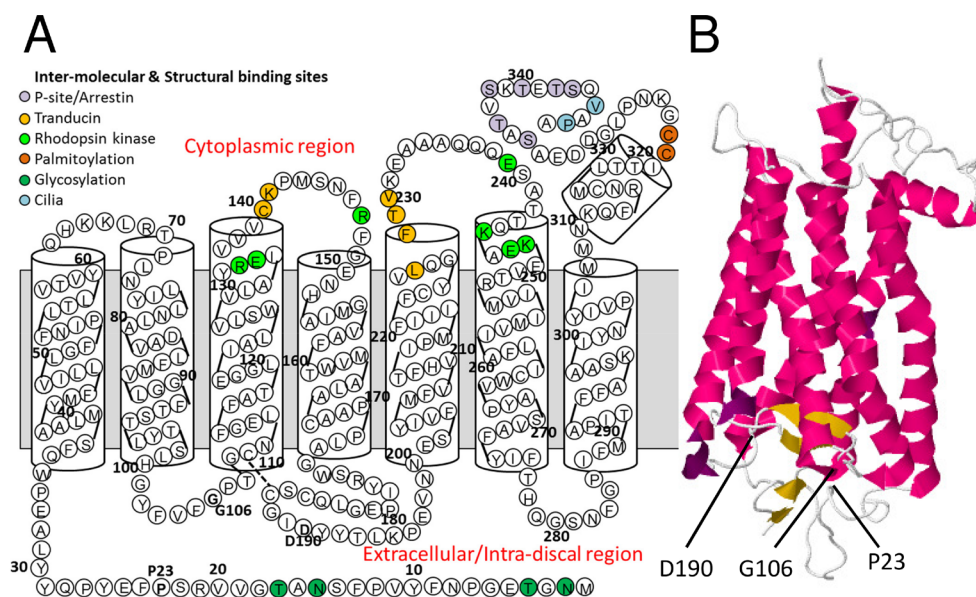

Figure 3. Rhodopsin structure. **A**: The position of each residue within a regional schematic of the trans-membrane helices, intradiscal regions, and cytoplasmic regions. Known specific residue functions are highlighted. The P23, G106, and D190 residues mutated by random site directed mutagenesis are annotated in bold (adapted from Rakoczy and Kiel [24]). **B**: The structure of rhodopsin showing the relative positions of the three residues mutagenized for in vitro analysis of surface expression, as determined with X-ray crystallography (RCSB reference 1U19 strand A, viewed using JMol). Figure 3A was adapted from a figure previously published in the *Journal of Molecular Biology* [24], Copyright Elsevier.
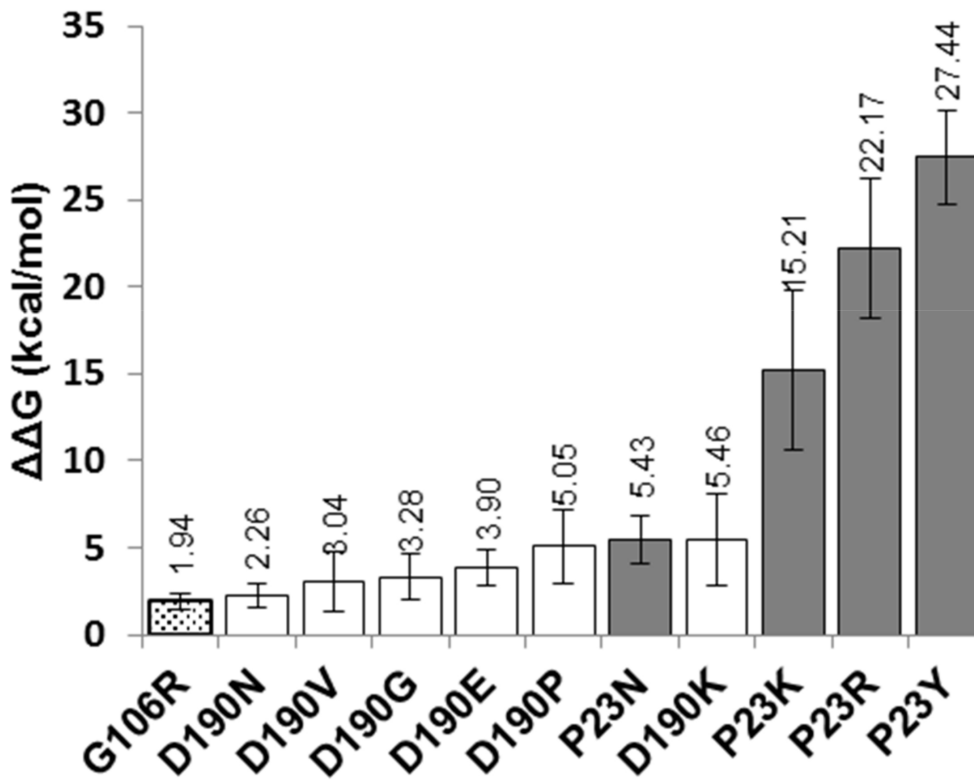
Figure 4. Stability of mutagenized rhodopsin variants. The plasmids generated by site-directed random mutagenesis show the relative change in free energy ($\Delta\Delta G$) that the mutation induces.
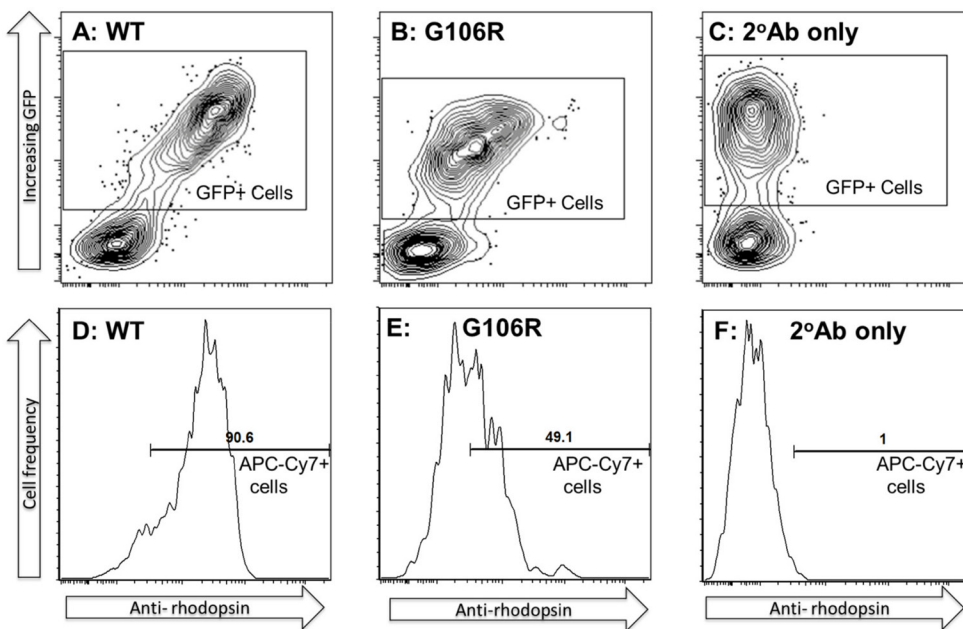

Figure 5. Flow cytometry of HEK-293 cells transfected with RHO-AC-mGFP. Top row: Flow cytometry allows one to investigate the relationship between total levels of rhodopsin (green fluorescent protein [GFP] intensity) and levels of rhodopsin at the cell surface (APC-Cy7). Here are shown wild-type transfections (**A**) and transfections of the G106R variant (**B**). A control sample treated with the secondary detection antibody alone (**C**) is shown for comparison of APC-Cy7 intensities. Two discrete populations can be seen in each culture, with transfected cells at high GFP levels (boxed region) versus non-transfected cells.

Bottom row: Histograms showing the relative intensity of rhodopsin expression at the cell surface (**D–E**) compared to controls treated with the secondary detection antibody alone (**F**).
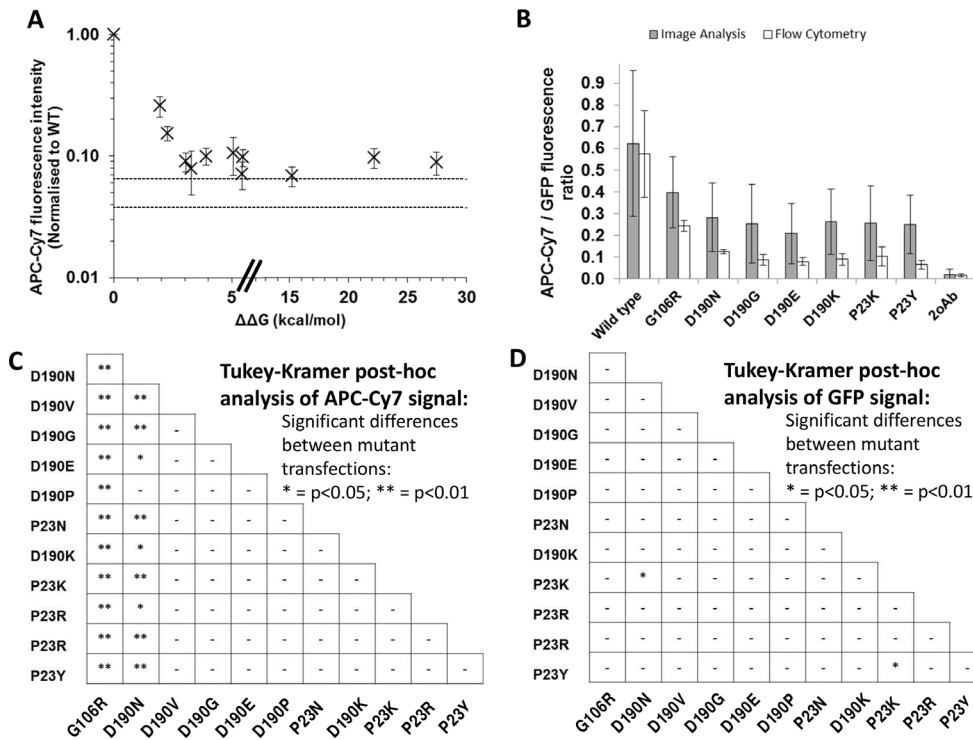
Figure 6. Correlation between rhodopsin variant stability and its presence at the cell surface. The relationship between the stability change predicted by FoldX and relative levels of membranous rhodopsin. **A**: APC-Cy7 fluorescence intensity of transfected cells normalized to wild-type. Data points represent means from five different transfections, error bars represent standard deviation, and the range of APC-Cy7 intensity produced by the secondary antibody control is shown between the two dotted horizontal lines. **B**: A comparison of the flow cytometry and image analysis data for examining the ratio between surface antibody signaling and the green fluorescent protein (GFP) signal. **C**: Tukey/Kramer post-hoc analysis of ANOVA analysis to examine the significance of the difference between wild-type normalized APC-cy7 and green fluorescent protein (GFP) ratios for the different mutant variants *=p<0.05; **=p<0.01. APC-Cy7 intensity showed a sharp drop at small stability changes. The surface expression of rhodopsin was significantly higher in the wild-type, G106R, and D190N than the other mutant variants, which expressed minimal levels of surface rhodopsin when $\Delta\Delta G$ was greater than D190N (2.26 kcal/mol). **D**: Tukey-Kramer post-hoc analysis of mutant GFP intensities, normalized to the wild-type. Overall, GFP intensity was more consistent between mutant transfections than was APC-Cy7 intensity. P23K transfections exhibited significantly lower GFP intensities than P23Y or D190N (p<0.05), but there were no other significant differences between any of the other variants in terms of GFP expression.

others=0.09±0.02 SD). The difference in the APC-Cy7 signal between D190P and the other more destabilized variants was not significant (Figure 6A,C).

There were some concerns that the drop in surface rhodopsin at high levels of destabilization may have been linked to the trypsinization process. However, a two-way ANOVA comparison between microscopy-based image analysis and flow cytometry showed that although the two methods resulted in significantly different ratios of surface antibody to GFP signal (p<0.01), the interaction effect between the data sets was not significant (p=0.9; see also Figure 6). This suggests that although the different antibodies and detection technologies caused an output shift, the size of the shift remained consistent for each mutant residue and so trypsinization did not affect these data.

Flow cytometry showed that there was a significant weakening of the overall GFP signal in all of the mutant variants compared to the wild type, but that there was little difference in the GFP intensity between the mutants (Figure 6). This would suggest that overall rhodopsin levels were reduced by even the mildest of changes to stability, but that further increases in $\Delta\Delta G$ between 1.94 and 27.44 kcal/mol did not have a compounding effect.

We followed the same strategy for statistical analysis of GFP intensity as we used to analyze APC-Cy7 data. ANOVA with repeated measures and Tukey-Kramer post-hoc analysis showed that the wild-type mean GFP intensity (2444.8 $_{RFI}$±1025.4 SD, n=5) was significantly higher (p<0.01) than any of the mutants (mutant means ranged from about 886 $_{RFI}$±453.1 SD for P23K to 1,549 $_{RFI}$±427.4 SD for P23Y). The mean GFP intensity for all mutants was 1316.5 $_{RFI}$±658.5 SD). A subsequent comparison of the normalized mutant/wild-type ratios (Figure 6D) revealed a marginally significant difference (p<0.05) between P23K (0.37 ±0.10) and both D190N (0.64 ±0.18 SD) and P23Y (0.67 ±0.13 SD), but there were no significant differences in the GFP signal intensity between any of the other mutants. The differences between the GFP intensities for the different variants were therefore

TABLE 5. PERCENTAGE OF CELLS WITH DETECTABLE SURFACE RHODOPSIN IN HEK-293 CULTURES TRANSFECTED WITH MUTANT RHODOPSIN VARIANTS.

Rhodopsin variant	ΔΔG (kcal/mol)	Mean % of transfected cells with detectable surface rhodopsin	S.D.
WT	0.00	89.4	13.6
G106R	1.94	71.2	13.9
D190N	2.26	41.7	9.7
D190V	3.04	17.4	7.1
D190G	3.28	27.9	20.5
D190E	3.90	27.5	14.6
D190P	5.05	23.2	10.3
P23N	5.43	15.8	7.5
D190K	5.46	24.9	11.9
P23K	15.21	13.0	2.5
P23R	22.17	18.9	6.3
P23Y	27.44	15.9	2.0

Comparison of molecular destabilization (ΔΔG) with surface rhodopsin frequencies for wild-type and mutant RHO-AC-mGFP plasmid transfections.

marginal and not as pronounced as they were between the equivalent APC-Cy7 intensities.

Cells transfected with the G106R plasmid, the mutation with the lowest ΔΔG at 1.94 kcal/mol, therefore retained the highest level of membrane-bound rhodopsin of any of the mutant variants. The D190N variant has the second lowest ΔΔG of any mutant variant (2.26 kcal/mol) and flow cytometry demonstrated a drastic drop in surface expression compared to G106R, but higher levels of surface rhodopsin than all of the other mutants.

Microscopy reflected the findings of flow cytometry to show that the least destabilizing mutations exhibited the highest levels of membranous rhodopsin. Surface rhodopsin was not evenly distributed throughout the plasma membrane of HEK-293 cells when transfected with the majority of mutant variants, but was expressed as small intense foci. In contrast, the wild-type, G106R, and D190N transfections demonstrated a more even distribution of surface expression, although D190N surface expression was present at greatly reduced levels. All mutants exhibited some expression of rhodopsin at the surface of the plasma membrane, but every mutant with the exception of G106R was associated with these small foci, even D190N, which also contained the more diffuse membranous protein in some cells.

A stark contrast between the wild-type, G106R, and other mutations was observed with confocal microscopy (Figure 7 and Figure 8). Cells transfected with the wild-type, the two human mutations G106R, D190N, and the most destabilizing

mutation (P23Y), were labeled with CD44 to determine the extent of colocalization between the GFP and this plasma membrane marker. As expected, the GFP and CD44 colocalized at high levels in the membranes of cells transfected with wild-type and G106R plasmids. Confocal microscopy also provided a clearer understanding of RHO-GFP localization in cells transfected with the D190N variant. All transfected cells showed high levels of cytoplasmic GFP, but some cells also showed even but low-level colocalization between CD44 and GFP at the plasma membrane.

DISCUSSION

The observed relationship between destabilization and the clinical data demonstrates the delicate balance of stability that governs the correct function of rhodopsin and its influence on the severity of retinal degeneration. This relationship highlights that in intradiscal residues, the effect of mutation-induced changes to rhodopsin stability has such a powerful impact that other structural/functional severity modifiers (such as interference with glycosylation or interaction motif activity) are masked by the stability change effects.

The high stability-severity correlation in the intradiscal region can be explained by referring to the work of Briscoe et al. [53], who found that sites containing disease-associated rhodopsin mutations with a lower expected chemical severity (ECS) are on average more critical to the protein's correct function than those with a high ECS. The intradiscal region has the lowest functionality of all of the regional
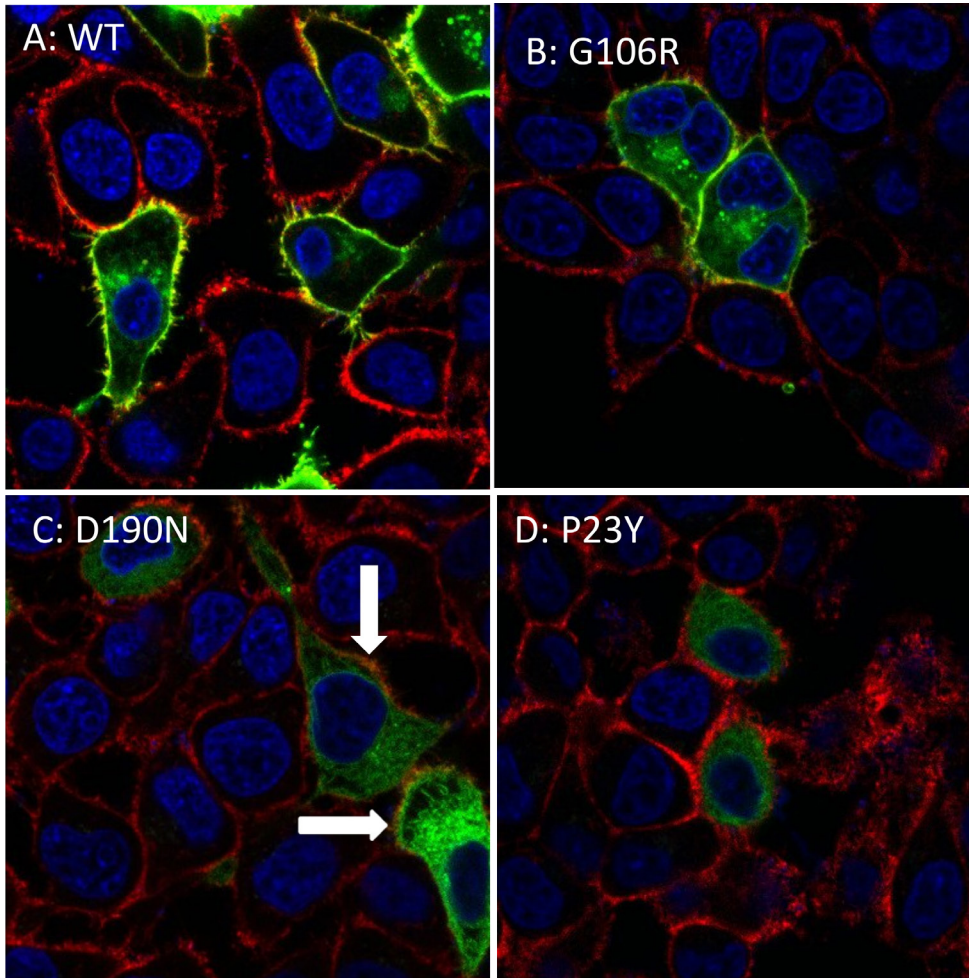
Figure 7. Rhodopsin expression at the cell surface HEK-293 cells transfected with rhodopsin-green fluorescent protein and stained with CD44 antibody, a marker of the cell surface. These images reflect the higher levels of surface rhodopsin in cells transfected with plasmids that express rhodopsin variants with low, rather than high, stability changes (**A**: Wild-type=0 kcal/mol. **B**: G106R=1.94 kcal/mol. **C**: D190n=2.26 kcal/mol. **D**: P23Y=27.44 kcal/mol). There were clearly higher levels of surface expression associated with the mildly destabilizing G106R mutation than with any of the other mutant variants. Unlike the wild-type and G106R mutant, the majority of the D190N rhodopsin remained in the cytoplasm, but in those cells where it was detected at the cell surface, there was a relatively even distribution (white arrows). This is in contrast to the other mutations, such as P23Y, which demonstrated low levels of surface rhodopsin that was restricted to discrete foci on the plasma membrane.

sub-categories. If a residue has a critical functional role, then factors other than destabilization will become the most important causes of molecular dysfunction. A minor change in structural stability could thus have a drastic effect on a functionally critical residue, and the relationship between ECS or stability and disease severity would be of less relevance to the disease status than the affected function. The respective functions of retinal-binding in the transmembranous region and the cilia trafficking, outer segment transport, and transmolecular interactions in the cytoplasmic region are thus all inhibited by less severe residue changes than are the intradiscal functions. It follows that there is less likely to be a correlation between stability and function in regions containing numerous residues with critical functions.

A hierarchy of functional importance may not provide the only explanation for the more robust correlation in the intradiscal residues, however. The correlation between disease severity and the destabilization level of intradiscal residues in this analysis was much more statistically robust than the correlation observed in the earlier function-excluded data set [24]. One possible explanation for this could be that the small size of the glycosylation sites in the intradiscal region relative to the protein-interaction sites of the other regions means that mutations close to the specific active residues would have a reduced conformational impact on these functions. It is also possible that the intradiscal domain plays a particularly important structural role for the molecule compared to the cytoplasmic domains: The four intradiscal domains are significantly associated with each other [54], and the central E2 intradiscal domain (see Figure 2) is particularly sensitive to the effects of mutation with 12 of the 26 residues mutated in RP [24]. Whatever the specific cause though, the importance of molecular destabilization relative to residue-specific interaction activity is increased in the intradiscal residues.

Another study has also generated multiple mutations in three residues of a single domain [55]. The transmembrane residues G121, A117, and G114 were each mutagenized seven
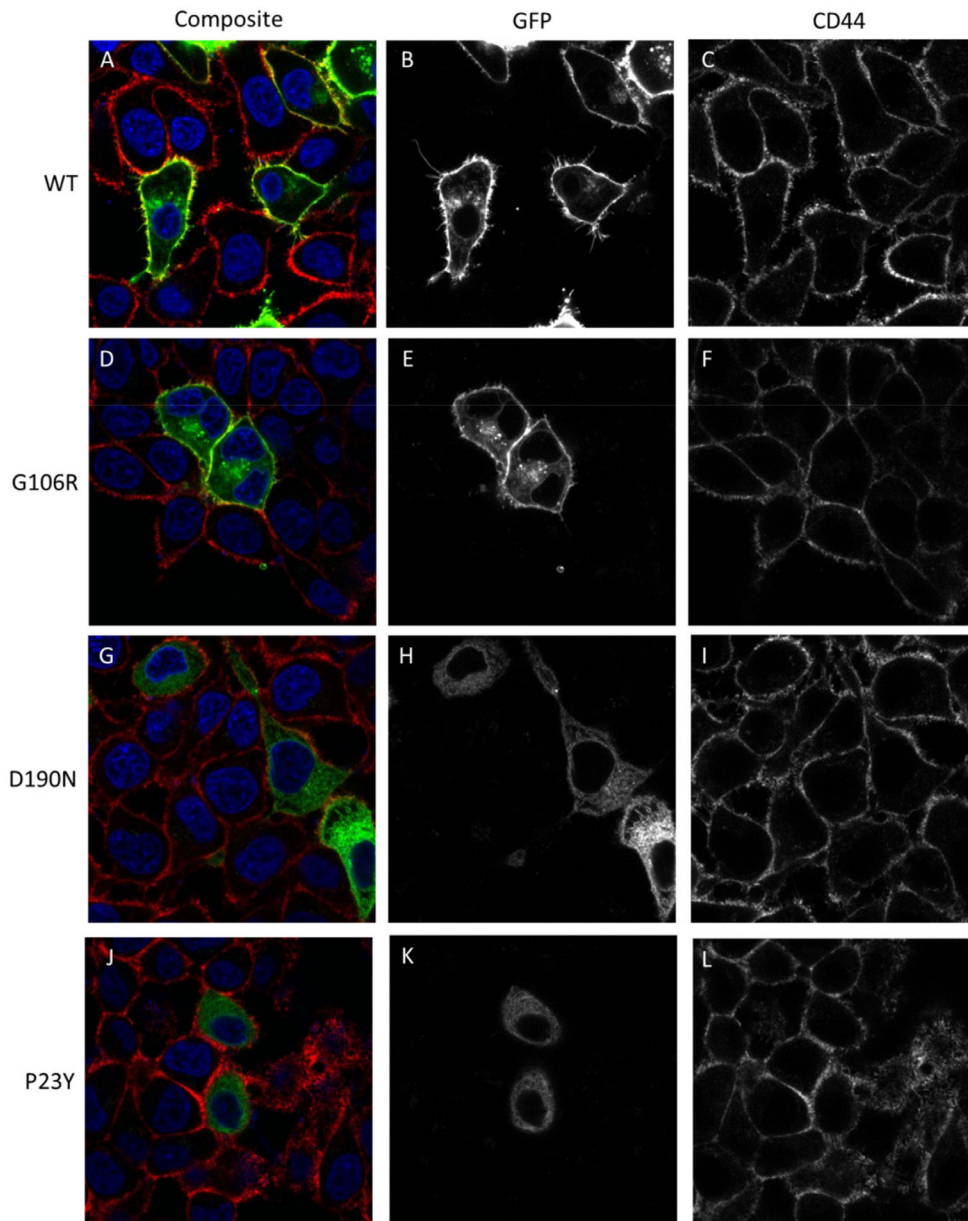
Figure 8. The expression of the rhodopsin-green fluorescent protein fusion protein in HEK-293 cells showing colocalization with the plasma membrane marker CD44 in the wild-type, G106R, and D190N but not P23Y transfections. Rhodopsin-green fluorescent protein (GFP; green) and CD44 (red) are presented as separate channels to show the full extent of colocalization. 4',6-Diamidino-2-phenylindole dihydrochloride (DAPI; blue) highlights the cell nuclei and is shown only in the composite images.

times to generate a cohort of 21 mutations. These residues are located on helix 3, the sub-domain that contains the counterion to the protonated Schiff's base at Lys296 that is formed by the binding of 11-cis retinal [56] and are thus within the retinal binding zone. This study showed a correlation between mutant residue size and the degree of blue-shift in the λ_{max} (wavelength of maximum absorbance) of the pigment. These findings are in agreement with our previous research that showed that the proximity of residues to retinal binding increases the severity of mutations [24].

Although there have been many previous reports of mutations that cause the internalization of rhodopsin within various cellular models [8-10,32], this is the first time that a quantitative method has shown a direct correlation between rhodopsin stability and its presence at the surface. The correlation is not surprising given that misfolded proteins are retained in the endoplasmic reticulum. However, the discovery of a quantifiable relationship between these two factors suggests that this approach might enable improvements to predictions of mutational effects. Using a transient transfection method rather than a stable transfection means that the rhodopsin sequence will be primarily expressed directly from the plasmid and there will be some expression variability caused by copy number and low-level genome

incorporation. However, we considered that the variability incurred by transient transfections would provide mean expression levels that are more consistent for comparisons of different variants than would the genomic incorporation at single sites resulting from stable transfections.

We expected that we might see a linear relationship between FoldX predictions of stability and the surface expression of rhodopsin. Instead, there was a threshold beyond which only minimal rhodopsin was transported toward the plasma membrane, giving rise to a sharp drop in total rhodopsin levels at low $\Delta\Delta G$. This means that the linear relationship observed between phenotype and stability must be influenced by additional stability-induced effects. Rhodopsin continuously undergoes rapid changes in morphology during the visual cycle, and thus, the nature of rhodopsin stability is more complex than simply maintaining enough stability to avoid misfolding and proteolysis. Some mutant variants are synthesized and transported correctly, but demonstrate aberrant behavior following multiple cycles of retinal isomerization and photobleaching [57]. Pathogenic mutations with moderate misfolding from the intradiscal region can be partially rescued by chaperones in vitro [58], but these rescued molecules tended to result in an increased level of metarhodopsin-I in relation to metarhodopsin-II, and an accumulation of aberrant photoproduct when subjected to prolonged illumination [58]. The relative stabilities of the different photointermediates are beyond the scope of this paper, but importantly, our method describes aspects of the core biosynthesis stability that allows the molecule to form at the ribosome and subsequently to maintain its conformation, thus allowing its release and transportation from the endoplasmic reticulum to the plasma membrane.

Our approach of integrating a literature-derived database with crystallography-based predictions of molecular stability and with flow cytometry has yielded data that support the view that the degree of rhodopsin destabilization has a powerful influence on disease severity. It has also highlighted a potential mechanism for this phenomenon and has shown that mutations in the intradiscal region are more likely to be amenable to severity predictions based on stability than are mutations in the other regions. There is a large variability in the severity of rhodopsin mutations, even between individuals who harbor the same mutation, and the intradiscal region is no exception. Indeed, the first mutation to be identified in humans (P23H) lies within the intradiscal region and is notoriously variable. Prognostic devices for rhodopsin-associated RP therefore cannot depend exclusively on genotype-based predictions and further characterization of the other contributing elements in this multifactorial disease are critical

if reliable and accurate prognoses are to ever be obtained. However, it is important to refine the interpretation of the genetic contribution as far as possible within these confines. Statistical means of severity based on genotype will certainly improve the current methods for estimating the severity of rare mutations. The estimated structural impact of any mutation has been shown to have potential as a valuable tool for practitioners and could be used for risk/benefit analysis of future treatment options.

REFERENCES

1. Stenson PD, Mort M, Ball EV, Howells K, Phillips AD, Thomas NS, Cooper DN. The Human Gene Mutation Database: 2008 update. Genome Med 2009; 1:13-[PMID: 19348700].

2. Richards JE, Scott KM, Sieving PA. Disruption of conserved rhodopsin disulfide bond by Cys187Tyr mutation causes early and severe autosomal dominant retinitis pigmentosa. Ophthalmology 1995; 102:669-77. [PMID: 7724183].

3. Berson EL. Long-term visual prognoses in patients with retinitis pigmentosa: the Ludwig von Sallmann lecture. Exp Eye Res 2007; 85:7-14. [PMID: 17531222].

4. Hartong DT, Berson EL, Dryja TP. Retinitis pigmentosa. Lancet 2006; 368:1795-809. [PMID: 17113430].

5. Besharse JC, Pfenninger KH. Membrane assembly in retinal photoreceptors I. Freeze-fracture analysis of cytoplasmic vesicles in relationship to disc assembly. J Cell Biol 1980; 87:451-63. [PMID: 7430251].

6. Chuang JZ, Zhao Y, Sung CH. SARA-regulated vesicular targeting underlies formation of the light-sensing organelle in mammalian rods. Cell 2007; 130:535-47. [PMID: 17693260].

7. Rajan RS, Illing ME, Bence NF, Kopito RR. Specificity in intracellular protein aggregation and inclusion body formation. Proc Natl Acad Sci USA 2001; 98:13060-5. [PMID: 11687604].

8. Saliba RS, Munro PM, Luthert PJ, Cheetham ME. The cellular fate of mutant rhodopsin: quality control, degradation and aggresome formation. J Cell Sci 2002; 115:2907-18. [PMID: 12082151].

9. Sung CH, Davenport CM, Nathans J. Rhodopsin mutations responsible for autosomal dominant retinitis pigmentosa. Clustering of functional classes along the polypeptide chain. J Biol Chem 1993; 268:26645-9. [PMID: 8253795].

10. Sung CH, Schneider BG, Agarwal N, Papermaster DS, Nathans J. Functional heterogeneity of mutant rhodopsins responsible for autosomal dominant retinitis pigmentosa. Proc Natl Acad Sci USA 1991; 88:8840-4. [PMID: 1924344].

11. Dryja TP, McGee TL, Reichel E, Hahn LB, Cowley GS, Yandell DW, Sandberg MA, Berson EL. A point mutation of the rhodopsin gene in one form of retinitis pigmentosa. Nature 1990; 343:364-6. [PMID: 2137202].

12. Kaushal S, Khorana HG. Structure and function in rhodopsin. 7. Point mutations associated with autosomal dominant retinitis pigmentosa. Biochemistry 1994; 33:6121-8. [PMID: 8193125].

13. Sung CH, Makino C, Baylor D, Nathans J. A rhodopsin gene mutation responsible for autosomal dominant retinitis pigmentosa results in a protein that is defective in localization to the photoreceptor outer segment. J Neurosci 1994; 14:5818-33. [PMID: 7523628].

14. Tam BM, Moritz OL, Hurd LB, Papermaster DS. Identification of an outer segment targeting signal in the COOH terminus of rhodopsin using transgenic Xenopus laevis. J Cell Biol 2000; 151:1369-80. [PMID: 11134067].

15. Frederick JM, Krasnoperova NV, Hoffmann K, Church-Kopish J, Ruther K, Howes K, Lem J, Baehr W. Mutant rhodopsin transgene expression on a null background. Invest Ophthalmol Vis Sci 2001; 42:826-33. [PMID: 11222546].

16. Sung CH, Davenport CM, Hennessey JC, Maumenee IH, Jacobson SG, Heckenlively JR, Nowakowski R, Fishman G, Gouras P, Nathans J. Rhodopsin mutations in autosomal dominant retinitis pigmentosa. Proc Natl Acad Sci USA 1991; 88:6481-5. [PMID: 1862076].

17. Mendes HF, van der Spuy J, Chapple JP, Cheetham ME. Mechanisms of cell death in rhodopsin retinitis pigmentosa: implications for therapy. Trends Mol Med 2005; 11:177-85. [PMID: 15823756].

18. Chuang JZ, Vega C, Jun W, Sung CH. Structural and functional impairment of endocytic pathways by retinitis pigmentosa mutant rhodopsin-arrestin complexes. J Clin Invest 2004; 114:131-40. [PMID: 15232620].

19. Zhu L, Jang GF, Jastrzebska B, Filipek S, Pearce-Kelling SE, Aguirre GD, Stenkamp RE, Acland GM, Palczewski K. A naturally occurring mutation of the opsin gene (T4R) in dogs affects glycosylation and stability of the G protein-coupled receptor. J Biol Chem 2004; 279:53828-39. [PMID: 15459196].

20. Andrés A, Garriga P, Manyosa J. Altered functionality in rhodopsin point mutants associated with retinitis pigmentosa.

Biochem Biophys Res Commun 2003; 303:294-301. [PMID: 12646201].

21. Rao VR, Cohen GB, Oprian DD. Rhodopsin mutation G90D and a molecular mechanism for congenital night blindness. Nature 1994; 367:639-42. [PMID: 8107847].

22. Anukanth A, Khorana HG. Structure and function in rhodopsin. Requirements of a specific structure for the intra-discal domain. J Biol Chem 1994; 269:19738-44. [PMID: 8051054].

23. Schymkowitz J, Borg J, Stricher F, Nys R, Rousseau F, Serrano L. The FoldX web server: an online force field. Nucleic Acids Res 2005; 33:W382–8-[PMID: 15980494].

24. Rakoczy EP, Kiel C, McKeone R, Stricher F, Serrano L. Analysis of disease-linked rhodopsin mutations based on structure, function, and protein stability calculations. J Mol Biol 2011; 405:584-606. [PMID: 21094163].

25. Guerois R, Nielsen JE, Serrano L. Predicting changes in the stability of proteins and protein complexes: a study of more than 1000 mutations. J Mol Biol 2002; 320:369-87. [PMID: 12079393].

26. Tokuriki N, Stricher F, Schymkowitz J, Serrano L, Tawfik DS. The stability effects of protein mutations appear to be universally distributed. J Mol Biol 2007; 369:1318-32. [PMID: 17482644].

27. Alibés A, Nadra AD, De Masi F, Bulyk ML, Serrano L, Stricher F. Using protein design algorithms to understand the molecular basis of disease caused by protein–DNA interactions: the Pax6 example. Nucleic Acids Res 2010; In press[PMID: 20685816].

28. Simões-Correia J, Figueiredo J, Lopes R, Stricher F, Oliveira C, Serrano L, Seruca R. E-cadherin destabilization accounts for the pathogenicity of missense mutations in hereditary diffuse gastric cancer. PLoS ONE 2012; 7:e33783-[PMID: 22470475].

29. Masica DL, Sosnay PR, Cutting GR, Karchin R. Phenotype-optimized sequence ensembles substantially improve prediction of disease-causing mutation in cystic fibrosis. Hum Mutat 2012; 33:1267-74.. [PMID: 22573477].

30. Pey AL, Stricher F, Serrano L, Martinez A. Predicted effects of missense mutations on native-state stability account for phenotypic outcome in phenylketonuria, a paradigm of misfolding diseases. Am J Hum Genet 2007; 81:1006-24. [PMID: 17924342].

31. Sergeev YV, Caruso RC, Meltzer MR, Smaoui N, MacDonald IM, Sieving PA. Molecular modeling of retinoschisin with functional analysis of pathogenic mutations from human X-linked retinoschisis. Hum Mol Genet 2010; 19:1302-13. [PMID: 20061330].

32. Rajan RS, Kopito RR. Suppression of wild-type rhodopsin maturation by mutants linked to autosomal dominant retinitis pigmentosa. J Biol Chem 2005; 280:1284-91. [PMID: 15509574].

33. Mao H, James T Jr, Schwein A, Shabashvili AE, Hauswirth WW, Gorbatyuk MS, Lewin AS. AAV delivery of wild-type

rhodopsin preserves retinal function in a mouse model of autosomal dominant retinitis pigmentosa. Hum Gene Ther 2011; 22:567-75. [PMID: 21126223].

34. Wilson JH, Wensel TG. The nature of dominant mutations of rhodopsin and implications for gene therapy. Mol Neurobiol 2003; 28:149-58. [PMID: 14576453].

35. Dobson CM. The structural basis of protein folding and its links with human disease. Philos Trans R Soc Lond B Biol Sci 2001; 356:133-45. [PMID: 11260793].

36. Dobson CM. Protein folding and misfolding. Nature 2003; 426:884-90. [PMID: 14685248].

37. Okada T, Sugihara M, Bondar AN, Elstner M, Entel P, Buss V. The retinal conformation and its environment in rhodopsin in light of a new 2.2 A crystal structure. J Mol Biol 2004; 342:571-83. [PMID: 15327956].

38. Altun A, Yokoyama S, Morokuma K. Spectral tuning in visual pigments: an ONIOM(QM:MM) study on bovine rhodopsin and its mutants. J Phys Chem B 2008; 112:6814-27. [PMID: 18473437].

39. Angel TE, Chance MR, Palczewski K. Conserved waters mediate structural and functional activation of family A (rhodopsin-like) G protein-coupled receptors. Proc Natl Acad Sci USA 2009; 106:8555-60. [PMID: 19433801].

40. Bhattacharya S, Hall SE, Vaidehi N. Agonist-induced conformational changes in bovine rhodopsin: insight into activation of G-protein-coupled receptors. J Mol Biol 2008; 382:539-55. [PMID: 18638482].

41. Stone EM, Kimura AE, Nichols BE, Khadivi P, Fishman GA, Sheffield VC. Regional distribution of retinal degeneration in patients with the proline to histidine mutation in codon 23 of the rhodopsin gene. Ophthalmology 1991; 98:1806-13. [PMID: 1775314].

42. Berson EL, Rosner B, Sandberg MA, Dryja TP. Ocular findings in patients with autosomal dominant retinitis pigmentosa and a rhodopsin gene defect (Pro-23-His). Arch Ophthalmol 1991; 109:92-101. [PMID: 1987956].

43. Berson EL, Sandberg MA, Dryja TP. Search for Correlations between Severity of Retinitis Pigmentosa and Primary Mutations. Digit J Ophthalmol 1998; 4:.

44. Niederhauser S, Mojon DS. Normal isopter position in the peripheral visual field in goldmann kinetic perimetry. Ophthalmologica 2002; 216:406-8. [PMID: 12566882].

45. Rasband WS. Image J. 1.41o ed. Bethesda, Maryland, USA: U.S. National Institute of Health. 2009

46. Chan F, Bradley A, Wensel TG, Wilson JH. Knock-in human rhodopsin-GFP fusions as mouse models for human disease and targets for gene therapy. Proc Natl Acad Sci USA 2004; 101:9109-14. [PMID: 15184660].

47. Jin S, McKee TD, Oprian DD. An improved rhodopsin/EGFP fusion protein for use in the generation of transgenic Xenopus laevis. FEBS Lett 2003; 542:142-6. [PMID: 12729914].

48. Moritz OL, Tam BM, Papermaster DS, Nakayama T. A functional rhodopsin-green fluorescent protein fusion protein localizes correctly in transgenic Xenopus laevis retinal rods and is expressed in a time-dependent pattern. J Biol Chem 2001; 276:28242-51. [PMID: 11350960].

49. Price BA, Sandoval IM, Chan F, Simons DL, Wu SM, Wensel TG, Wilson JH. Mislocalization and degradation of human P23H-rhodopsin-GFP in a knockin mouse model of retinitis pigmentosa. Invest Ophthalmol Vis Sci 2011; 52:9728-36. [PMID: 22110080].

50. Sanchis J, Fernandez L, Carballeira JD, Drone J, Gumulya Y, Hobenreich H, Kahakeaw D, Kille S, Lohmer R, Peyralans JJ, Podtetenieff J, Prasad S, Soni P, Taglieber A, Wu S, Zilly FE, Reetz MT. Improved PCR method for the creation of saturation mutagenesis libraries in directed evolution: application to difficult-to-amplify templates. Appl Microbiol Biotechnol 2008; 81:387-97. [PMID: 18820909].

51. Illing ME, Rajan RS, Bence NF, Kopito RR. A rhodopsin mutant linked to autosomal dominant retinitis pigmentosa is prone to aggregate and interacts with the ubiquitin proteasome system. J Biol Chem 2002; 277:34150-60. [PMID: 12091393].

52. Zhang B, Shan H, Li D, Li ZR, Zhu KS, Jiang ZB, Huang MS. Different methods of detaching adherent cells significantly affect the detection of TRAIL receptors. Tumori 2012; 98:800-3. [PMID: 23389369].

53. Briscoe AD, Gaur C, Kumar S. The spectrum of human rhodopsin disease mutations through the lens of interspecific variation. Gene 2004; 332:107-18. [PMID: 15145060].

54. Okada T, Ernst OP, Palczewski K, Hofmann KP. Activation of rhodopsin: new insights from structural and biochemical studies. Trends Biochem Sci 2001; 26:318-24. [PMID: 11343925].

55. Han M, Lin SW, Smith SO, Sakmar TP. The effects of amino acid replacements of glycine 121 on transmembrane helix 3 of rhodopsin. J Biol Chem 1996; 271:32330-6. [PMID: 8943295].

56. Ridge KD, Abdulaev NG, Sousa M, Palczewski K. Phototransduction: crystal clear. Trends Biochem Sci 2003; 28:479-87. [PMID: 13678959].

57. Toledo D, Ramon E, Aguila M, Cordomi A, Perez JJ, Mendes HF, Cheetham ME, Garriga P. Molecular mechanisms of disease for mutations at Gly-90 in rhodopsin. J Biol Chem 2011; 286:39993-40001. [PMID: 21940625].

58. Krebs MP, Holden DC, Joshi P, Clark CL 3rd, Lee AH, Kaushal S. Molecular mechanisms of rhodopsin retinitis pigmentosa and the efficacy of pharmacological rescue. J Mol Biol 2010; 395:1063-78. [PMID: 19913029].

59. van den Born LI, van Schooneveld MJ, de Jong LA, Riemslag FC, de Jong PT, Gal A, Bleeker-Wagemakers EM. Thr4Lys rhodopsin mutation is associated with autosomal dominant retinitis pigmentosa of the cone-rod type in a small Dutch family. Ophthalmic Genet 1994; 15:51-60. [PMID: 7850269].

60. Sullivan LJ, Makris GS, Dickinson P, Mulhall LE, Forrest S, Cotton RG, Loughnan MS. A new codon 15 rhodopsin gene mutation in autosomal dominant retinitis pigmentosa is

associated with sectorial disease. Arch Ophthalmol 1993; 111:1512-7. [PMID: 8240107].

61. Bell C, Converse CA, Hammer HM, Osborne A, Haites NE. Rhodopsin mutations in a Scottish retinitis pigmentosa population, including a novel splice site mutation in intron four. Br J Ophthalmol 1994; 78:933-8. [PMID: 7819178].

62. Fishman GA, Stone EM, Sheffield VC, Gilbert LD, Kimura AE. Ocular findings associated with rhodopsin gene codon 17 and codon 182 transition mutations in dominant retinitis pigmentosa. Arch Ophthalmol 1992; 110:54-62. [PMID: 1731723].

63. Hayakawa M, Hotta Y, Imai Y, Fujiki K, Nakamura A, Yanashima K, Kanai A. Clinical features of autosomal dominant retinitis pigmentosa with rhodopsin gene codon 17 mutation and retinal neovascularization in a Japanese patient. Am J Ophthalmol 1993; 115:168-73. [PMID: 7679248].

64. Jacobson SG, Kemp CM, Sung CH, Nathans J. Retinal function and rhodopsin levels in autosomal dominant retinitis pigmentosa with rhodopsin mutations. Am J Ophthalmol 1991; 112:256-71. [PMID: 1882937].

65. Schuster A, Weisschuh N, Jagle H, Besch D, Janecke AR, Zierler H, Tippmann S, Zrenner E, Wissinger B. Novel rhodopsin mutations and genotype-phenotype correlation in patients with autosomal dominant retinitis pigmentosa. Br J Ophthalmol 2005; 89:1258-64. [PMID: 16170112].

66. Oh KT, Weleber RG, Lotery A, Oh DM, Billingslea AM, Stone EM. Description of a New Mutation in Rhodopsin, Pro23Ala, and Comparison With Electroretinographic and Clinical Characteristics of the Pro23His Mutation. Arch Ophthalmol 2000; 118:1269-76. [PMID: 10980774].

67. Heckenlively JR, Rodriguez JA, Daiger SP. Autosomal dominant sectoral retinitis pigmentosa. Two families with transversion mutation in codon 23 of rhodopsin. Arch Ophthalmol 1991; 109:84-91. [PMID: 1987955].

68. Kemp CM, Jacobson SG, Roman AJ, Sung CH, Nathans J. Abnormal rod dark adaptation in autosomal dominant retinitis pigmentosa with proline-23-histidine rhodopsin mutation. Am J Ophthalmol 1992; 113:165-74. [PMID: 1550184].

69. Bareil C, Hamel C, Pallares-Ruiz N, Arnaud B, Demaille J, Claustres M. Molecular analysis of the rhodopsin gene in southern France: identification of the first duplication responsible for retinitis pigmentosa, c.998999ins4. Ophthalmic Genet 1999; 20:173-82. [PMID: 10521250].

70. Fishman GA, Stone EM, Gilbert LD, Sheffield VC. Ocular findings associated with a rhodopsin gene codon 106 mutation. Glycine-to-arginine change in autosomal dominant retinitis pigmentosa. Arch Ophthalmol 1992; 110:646-53. [PMID: 1580841].

71. Moore AT, Fitzke FW, Kemp CM, Arden GB, Keen TJ, Inglehearn CF, Bhattacharya SS, Bird AC. Abnormal dark adaptation kinetics in autosomal dominant sector retinitis pigmentosa due to rod opsin mutation. Br J Ophthalmol 1992; 76:465-9. [PMID: 1390527].

72. Goliath R, Bardien S, September A, Martin R, Ramesar R, Greenberg J. Rhodopsin mutation G109R in a family with autosomal dominant retinitis pigmentosa. Hum Mutat 1998; Suppl 1S40-1. [PMID: 9452035].

73. Antiñolo G, Sanchez B, Borrego S, Rueda T, Chaparro P, Cabeza JC. Identification of a new mutation at codon 171 of rhodopsin gene causing autosomal dominant retinitis pigmentosa. Hum Mol Genet 1994; 3:1421-[PMID: 7987326].

74. Fishman GA, Vandenburgh K, Stone EM, Gilbert LD, Alexander KR, Sheffield VC. Ocular findings associated with rhodopsin gene codon 267 and codon 190 mutations in dominant retinitis pigmentosa. Arch Ophthalmol 1992; 110:1582-8. [PMID: 1444916].

75. Cideciyan AV, Hood DC, Huang Y, Banin E, Li ZY, Stone EM, Milam AH, Jacobson SG. Disease sequence from mutant rhodopsin allele to rod and cone photoreceptor degeneration in man. Proc Natl Acad Sci USA 1998; 95:7103-8. [PMID: 9618546].

76. Kranich H, Bartkowski S, Denton MJ, Krey S, Dickinson P, Duvigneau C, Gal A. Autosomal dominant 'sector' retinitis pigmentosa due to a point mutation predicting an Asn-15-Ser substitution of rhodopsin. Hum Mol Genet 1993; 2:813-4. [PMID: 8353500].

77. Sheffield VC, Fishman GA, Beck JS, Kimura AE, Stone EM. Identification of novel rhodopsin mutations associated with retinitis pigmentosa by GC-clamped denaturing gradient gel electrophoresis. Am J Hum Genet 1991; 49:699-706. [PMID: 1897520].